(Received 16 October 2025, Accepted 5 December 2025, Scheduled 15 January 2026)

Design of a High Gain Low SAR Microstrip Antenna Array with AMC Structure for Wearable Applications

Jialin Zhang, Cheng-Zhu Du*, and Xu Wu

College of Electronics and Information Engineering, Shanghai University of Electric Power, Shanghai 200090, China

ABSTRACT: In this paper, a novel wearable antenna array backed by an AMC reflector is presented for high gain and low side-lobe levels. The presented antenna consists of a four-element array. The impedance bandwidth (≤ -10 dB) of the proposed antenna is from 5.6 to 6.8 GHz. After adding an AMC structure on the back side of the antenna array, the maximum measured gain reaches 13.8 dBi at 6.7 GHz; the front-to-back ratio (FBR) value is raised by 25.3 dB; and the sidelobe level is less than -20.51 dB. When the antenna array is on the human body model, the simulated SAR value is only 0.05 W/Kg/10 g, significantly lower than the international standard. These good measured results demonstrate that the proposed antenna is suitable for modern wearable applications.

1. INTRODUCTION

In recent years, the rapid advancement of 5G technology [1–3], with its extensive coverage, high speed, and low latency, has expanded application scenarios for satellite communications. Meanwhile, the global coverage and mobility of satellite communications [4], in turn, complement 5G networks. The integration of these two technologies will become a significant trend [5, 6], driving the widespread application of the Internet of Things (IoT) [7, 8]. Besides, the 5G NTN (Non-Terrestrial Network) standard propels integrated space — terrestrial communications, with wearable devices emerging as a significant terminal. The technology of Body Area Networks (BANs) enables seamless communication between wearable devices and other IoT systems [9].

Loading electromagnetic band gap (EBG) [10–12], artificial magnetic conductor (AMC) [13–19], and frequency selective surface(FSS) [20] structures behind wearable antennas is a common technique to enhance gain and reduce radiation exposure to the human body. In [10], by adding an EBG structure, the antenna gain is increased from 2.46 dBi to 6.75 dBi, the FBR improved to over 13.82 dB, and the specific absorption rate (SAR) reduced by approximately 90%. The zero-phase reflection boundary of the AMC reconfigures the antenna's current distribution. The AMC surface sustains a $\lambda/2$ resonance within the target band, tuning its reflection phase to 0° and ensuring the reflected wave in-phase with the incident wave. This suppresses backward coupling toward the body and transforms it into in-phase radiation, resulting in concurrent gain enhancement and SAR reduction. An AMC-backed antenna on a leather substrate is achieved around 90% SAR reduction [16]. A unit antenna exhibits a 75% gain increase and 99.5% lower SAR after introducing an AMC reflector [17]. The efficacy of an AMC structure for improving multiband antenna performance is validated by [18]. At the center frequencies of 1.8 GHz, 2.45 GHz, and 3.5 GHz, respective gain increases of 3.4 dBi, 1.8 dBi, and 4.0 dBi are observed. However, these studies are all based on single-element antennas, with the highest gain reaching only 7.9 dB. Employing array antennas can achieve a more significant gain enhancement with less effort. In [19], the proposed antenna incorporates an AMC-backed four-element array, achieving a gain of 12.03 dB and FBR of 26.04 dB. In [20], a 1×4 antenna array loaded with an FSS structure has been proposed, and the peak gain is 12.4 dB. In [21], the proposed antenna array employs a bottom-loaded uniplanar compact electromagnetic band gap (UC-EBG) structure, realizing a gain of 13.6 dB and side-lobe level less than -12 dB. A low side lobe reduces multipath interference during signal transmission, improving communication link reliability and signal-to-noise ratio. As a result, a low side-lobe wearable antenna can minimize unnecessary electromagnetic radiation towards other parts of the human body or nearby electronic devices. Therefore, it is a hard work to design the wearable antenna array with high gain, low side lobe, low SAR, and high front-to-back ratio (FBR).

In this paper, a wearable antenna array backed by an AMC structure is proposed for high gain and low side-lobe levels. The final overall antenna array size is 122 mm $\times$ 48.8 mm. The measured bandwidth is from 5.6 GHz to 6.8 GHz. With the backed AMC structure, the antenna acquires the measured maximum gain of 13.8 dBi and an FBR value of 25.3 dB, and the measured side-lobe level is less than -18.5 dB. At the same time, the simulated SAR value is only 0.05 W/kg at 6.5 GHz.

The innovations in the paper are: the antenna array is integrated with an AMC reflector, achieving the good performance of high gain, low side-lobe level, high FBR, and low SAR, which is suitable for wearable applications.

* Corresponding author: Chengzhu Du (duchengzhu@163.com).

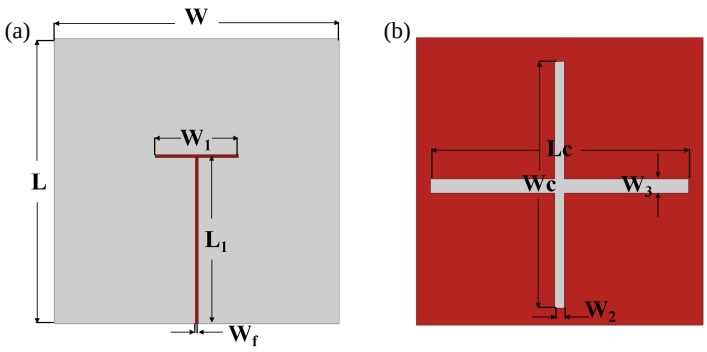

FIGURE 1. Illustration of the antenna element structure: (a) top view; (b) back view.

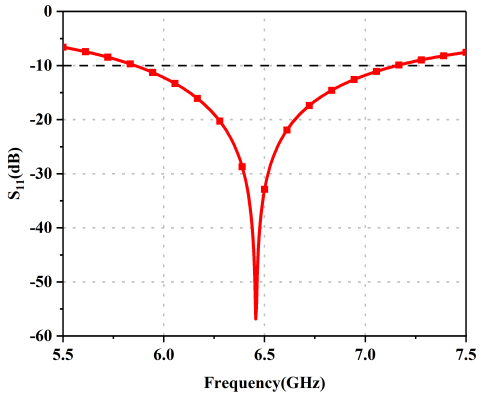

FIGURE 2. S_{11} of unit antenna.

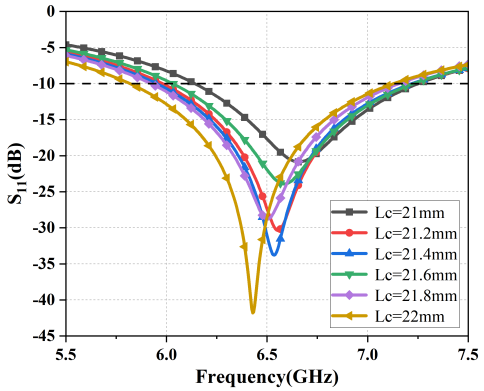

FIGURE 3. The influence of L_c on S_{11}.

2. ANTENNA DESIGN AND CONFIGURATION

2.1. Antenna Element Design

The layout of the antenna element is illustrated in Figure 1. A flexible liquid crystal polymer (LCP) layer is used as the dielectric substrate, characterized by a loss tangent of 0.002 and a dielectric constant of 2.9. On the top side of the antenna is a T-shaped feeder, and a cruciform slot is etched onto the backside of the antenna's ground plane to provide proper impedance matching. The overall size of the antenna unit is 24 mm × 24 mm × 0.1 mm. Table 1 summarizes the detailed dimensions of the antenna.

TABLE 1. Antenna dimensions.

Dimension	Value (mm)	Dimension	Value (mm)
W	24	L	24
W_1	7	L_1	14
L_c	21.6	W_c	20.6
W_3	1.2	W_2	0.8
W_f	0.26		

The simulated S_{11} parameter of the antenna element is presented in Figure 2, and the operating frequency band of the antenna covers 5.86–7.16 GHz, including the fixed satellite service frequency band (6.425–6.725 GHz). Figure 3 illustrates the influence of the length L_c on the performance of S_{11}. As L_c increases, the antenna's S_{11} shifts to lower frequencies. A series of simulations were conducted to optimize the design. To preserve the high-frequency performance of the antenna, $L_c = 21.6$ mm was chosen as it represents a compromise that yields the optimal impedance matching.

2.2. Antenna Array Design

Figure 4 shows a 1×4 antenna array consisting of four antenna units connected by a 1×4 power divider. The spacing between the antenna units is 26.2 mm. The Chebyshev unequal-spacing algorithm is utilised in the design of the power divider to achieve an optimum amplitude distribution. The nonuniform amplitude distribution obtained through this approach effectively reduces side-lobe levels. This synthesis method achieves optimal radiation pattern performance while maintaining main-lobe beamwidth. The total physical dimensions of the antenna are given as 103.24 mm × 30 mm. Figure 5 presents the simulated S parameters of the 1-to-4 unequal power divider. Simulation results indicate that the operating bandwidth of the power divider covers 2.11–9 GHz, with an inter-port isolation better than −3 dB across the band.

Figure 6(a) is the S_{11} of antenna array, which covers 6.05 to 6.92 GHz. The mutual coupling between antenna elements leads to a reduction in the relative bandwidth of the antenna array. The radiation pattern at 6.5 GHz is shown in Figure 6(b). The E-plane is yoz plane, and the H-plane is xoz plane. Figure 7 presents the simulated far-field radiation pattern of an un-

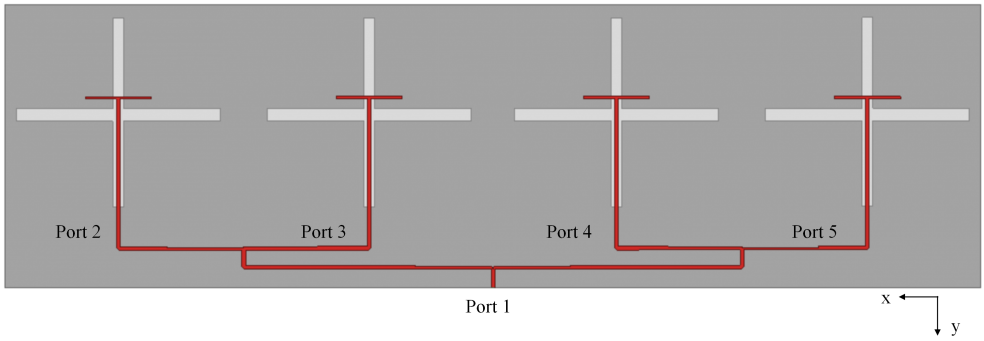

FIGURE 4. Antenna array structure.

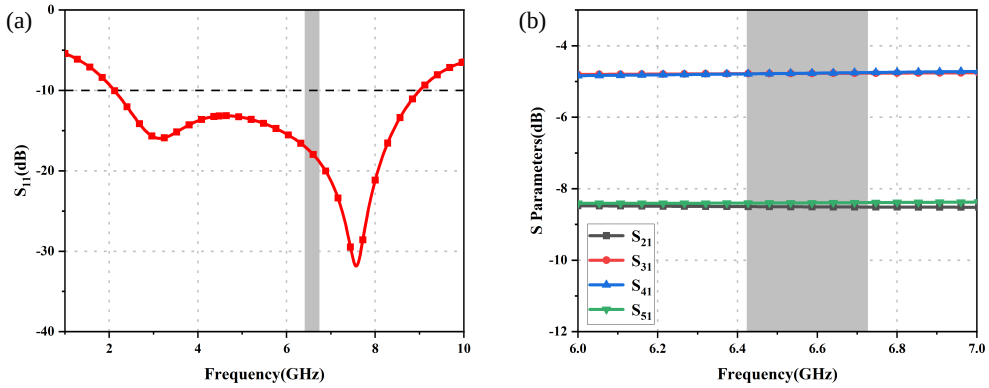

FIGURE 5. S parameters of the 1-to-4 power divider. (a) S_{11} parameter. (b) Port-to-port isolation.

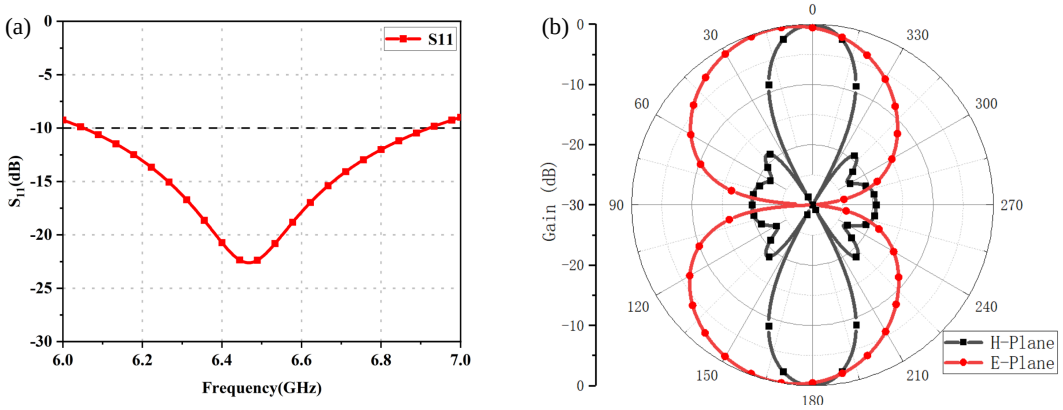

FIGURE 6. Antenna array performance. (a) S_{11} parameter. (b) Radiation pattern at 6.5 GHz

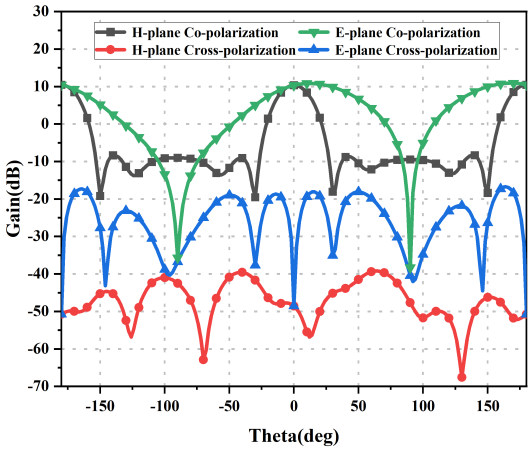

FIGURE 7. Radiation pattern of the antenna array.

equally spaced four-element array at 6.5 GHz. It can be seen that the antenna array achieves a realized gain of 10.94 dB, and the first side-lobe level is below −19.2 dB. Additionally, the cross-polarization gain of the antenna is significantly lower than the co-polarization gain, indicating good radiation performance.

2.3. AMC Array Design

In order to improve the gain and FBR of the antenna, an AMC reflector is proposed to be placed at the bottom of the antenna. The size of AMC structure can refer to the following equation:

$$L = \mu_0 t \tag{1}$$

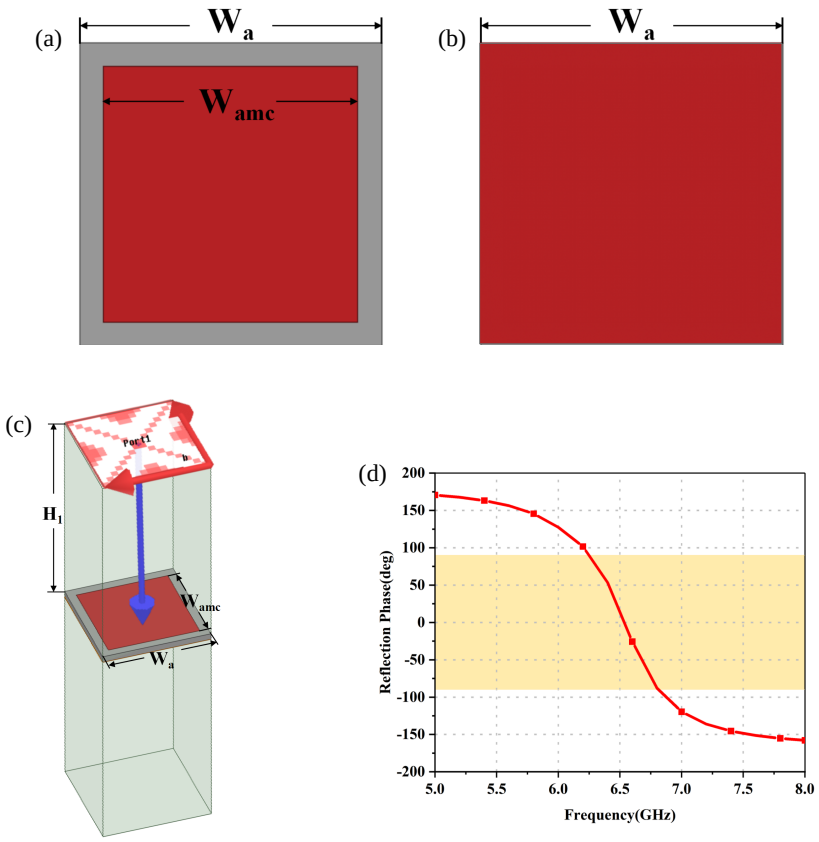

FIGURE 8. The proposed AMC element. (a) Top view. (b) Back view. (c) The boundary conditions for unit cell. (d) Reflection phase of the proposed AMC element.

$$C = \frac{\varepsilon_0 (1+\varepsilon_r) w}{\pi} \cos h^{-1}\left(\frac{2w+g}{g}\right) \tag{2}$$

$$f_0 = \frac{1}{2\pi\sqrt{LC}} \tag{3}$$

In this context, L and C represent inductance and capacitance; ε_r is the dielectric constant of the substrate; ε_0 is the dielectric constant of free space; w is the length of the patch; g is the distance between the AMC patch; μ_0 is the permeability of the dielectric substrate; t is the dielectric substrate's thickness; f_0 is the operating frequency of the AMC structure.

Figures 8(a) and 8(b) present the layout of the designed AMC element. The AMC element uses a 0.813 mm thick semi-flexible Rogers 4003C as the dielectric substrate, with a dielectric constant of 3.38 and a loss tangent of 0.0027. The parameters W_a and W_{amc} are assigned the values of 13.2 mm and 11.12 mm, respectively. The system is excited using a waveguide port placed on the top of the waveguide as shown in Figure 8(c). The reflection phase was measured at a distance of $H_1 = \lambda/4$ from the AMC surface, where λ is the wavelength at the target frequency. Figure 8(d) shows the reflection phase of the proposed AMC element. The AMC bandwidth of the reflection phase between $-90°$ and $+90°$ is maintained over the 6.25–6.81 GHz frequency span.

Figure 9 presents the complete topology of the antenna array integrated with the AMC reflector, and the 10×4 AMC array is loaded beneath the antenna array, with an air gap of 4.25 mm

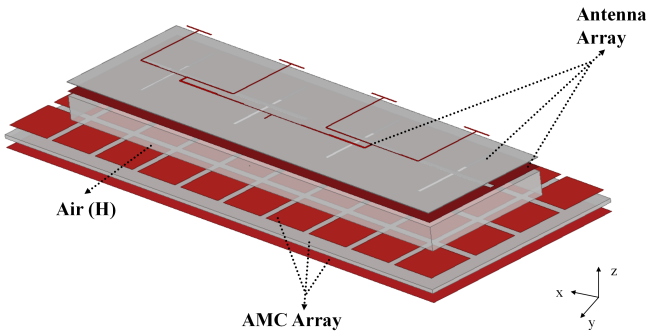

FIGURE 9. Layout of the antenna array with an AMC reflector.

separating the two layers. The overall dimensions of the integrated antenna array are 122 mm $\times$48.8 mm.

Figure 10 compares the S_{11} curves of the antenna with and without the AMC structure. After loading the AMC, the antenna's bandwidth is slightly reduced, with the -10 dB bandwidth ranging from 6.3 to 6.77 GHz. The bandwidth of the antenna covers the C-band satellite communication frequency range of 6.425 to 6.725 GHz. Figure 11 presents a comparison between the measured and simulated radiation efficiencies of the antenna. The radiation efficiency remains above 80% across the operating frequency band, indicating good radiation characteristics of the antenna.

Figure 12 compares the 6.5 GHz radiation patterns for the antenna design with and without the AMC. A notable suppression of backward radiation is observed when the AMC is incorpo-

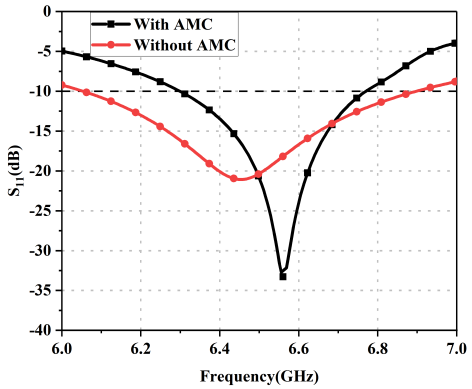

FIGURE 10. S_{11} of the antenna with and without the AMC structure.

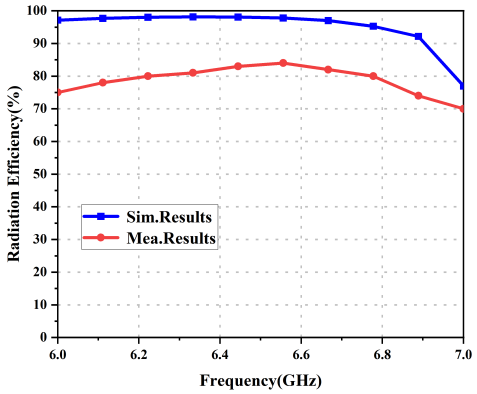

FIGURE 11. Measured and simulated radiation efficiencies.

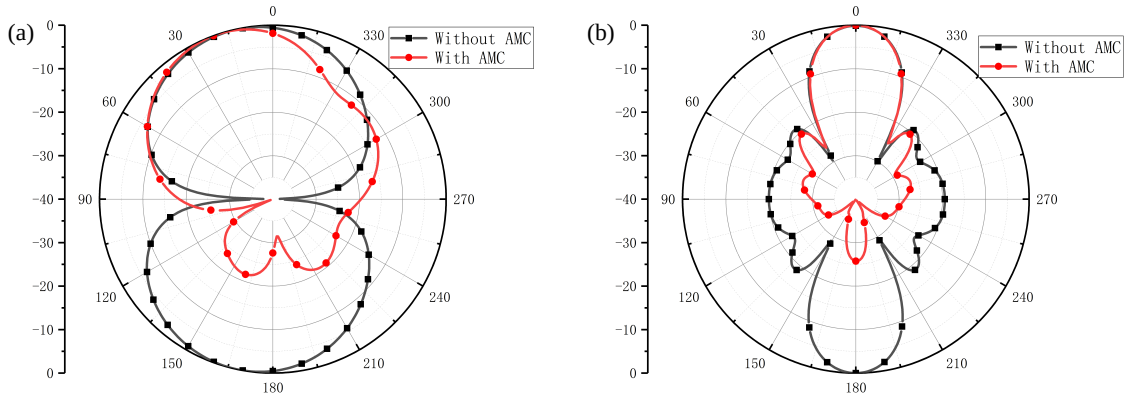

FIGURE 12. Radiation pattern comparison at 6.5 GHz: With vs. Without AMC. (a) yoz plane. (b) xoz plane.

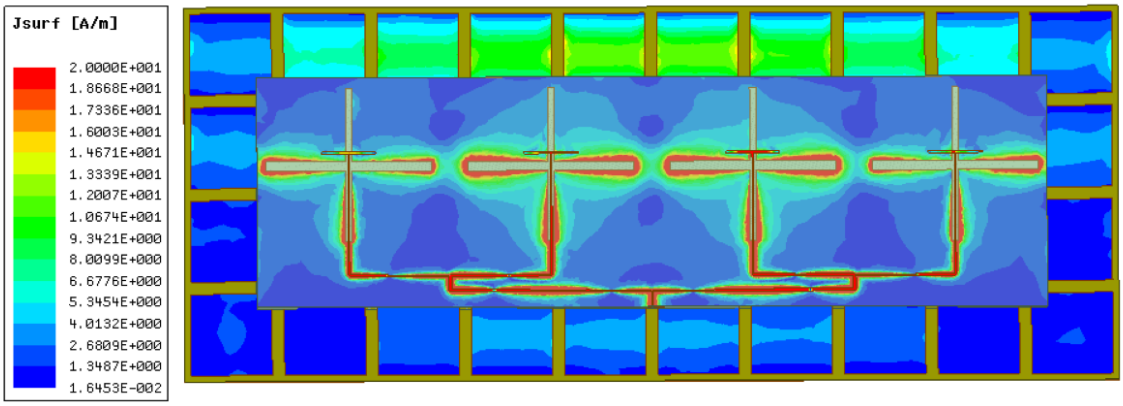

FIGURE 13. The distribution of surface current on the antenna.

rated. By adding AMC reflector, the side-lobe level decreases to -20.51 dB, and the FBR attains a value of 25.3 dB. Besides, a maximum gain of 14.43 dB is achieved with the AMC loaded, representing an enhancement of 3.49 dB over the original design.

Figure 13 illustrates the current distribution of the AMC antenna array. The induced current flows predominantly along the antenna array's uppermost transmission line and the gaps in the bottom ground plane.

The impact of varying the separation between the antenna and AMC layer on both S_{11} and radiation pattern is presented in Figure 14. As the AMC distance H increases, the antenna's bandwidth shifts to high frequencies, and the side-lobe level rises slightly. The antenna performs the best when H is 4.25 mm.

Table 2 shows the performance comparison of the antenna after loading AMC arrays of different sizes. As shown in the table, when a larger AMC reflector is loaded, the antenna gain is higher. Therefore, after a comprehensive trade-off among gain, side-lobe level, and overall size, a 10×4 AMC array was selected as the optimal configuration.

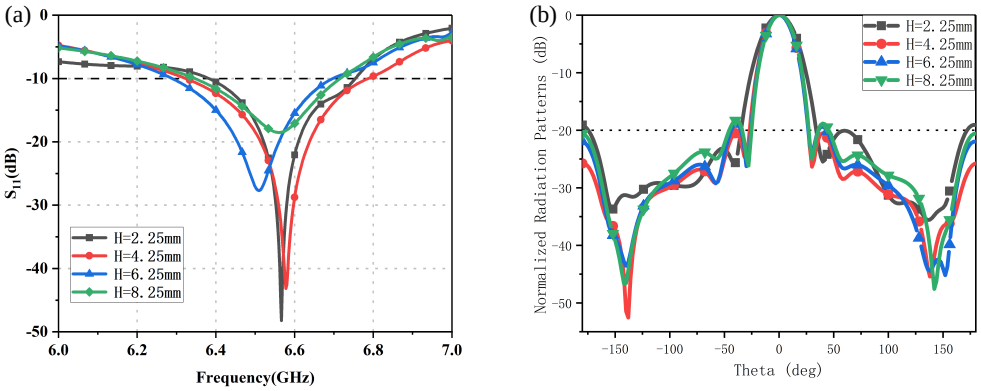

FIGURE 14. The effect of H on S_{11} parameter and radiation pattern. (a) S_{11} parameter. (b) Radiation pattern.

TABLE 2. Antenna performance with varied numbers of AMC elements.

AMC unit layout	Frequency (GHz)	Side Lobe (dB)	Gain (dB)
9×3	6.23–6.89	−19.9	13.8
10×4	6.3–6.77	−20.51	14.44
12×5	6.3–6.78	−19.39	14.5

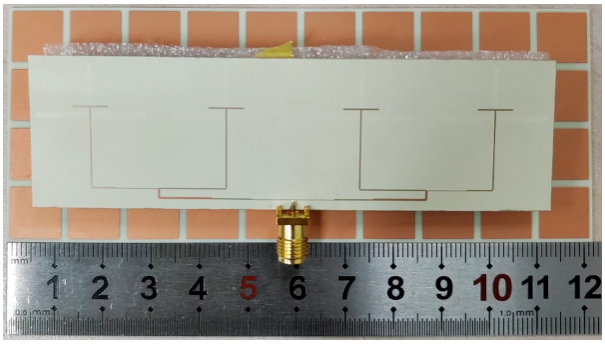

FIGURE 15. Fabricated antenna prototype.

3. MEASURED RESULTS AND ANALYSIS

3.1. S-Parameters

Figure 15 presents a photograph of the fabricated antenna. The S-parameters were measured by an Agilent Technologies E8363C vector network analyzer. Figure 16 compares the measured and simulated S_{11} results for the antenna array with the AMC reflector. Due to the influence of measurement environment and manufacturing tolerances, the measured bandwidth ranges from 5.6 to 6.8 GHz, which is 600 MHz wider than the simulation and fully covers the simulated bandwidth. Moreover, the resonant frequencies corresponding to the minimum S_{11} are consistent.

In Figure 17, the antenna's wearable performance was assessed on the human body at different on-body locations, namely the chest, leg, and arm. As shown in Figure 17, the measured S_{11} parameters demonstrate that the antenna effectively maintains its required frequency range when being worn on the body. The designed antenna is curved along

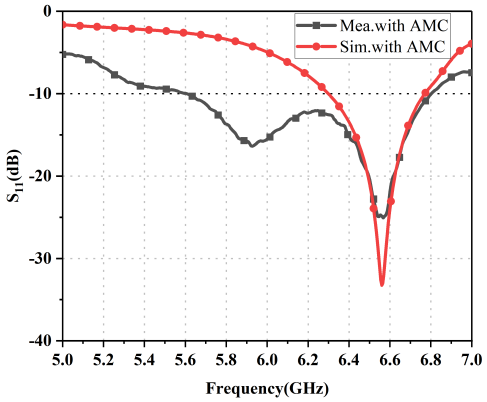

FIGURE 16. The measured and simulated S_{11} of the antenna with AMC reflector.

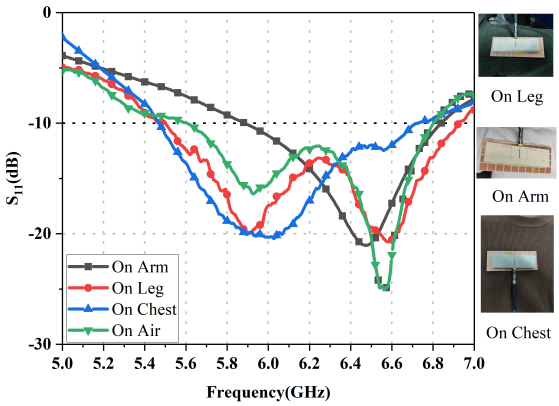

FIGURE 17. Measured S_{11} parameters on different body parts.

the cylinder, which has a radius of 160 mm. As shown in Figure 18, the S_{11} parameter of the bent antenna shows a smoother profile in the lower band. Staying below −10 dB, the bandwidth of bending condition is wider than the flat condition, while still satisfying the operational requirements.

3.2. Far-Field Radiation

The far-field measurement setup is depicted in Figure 19. The far-field measurements were conducted in a microwave anechoic chamber. A comparison between the simulated and mea-

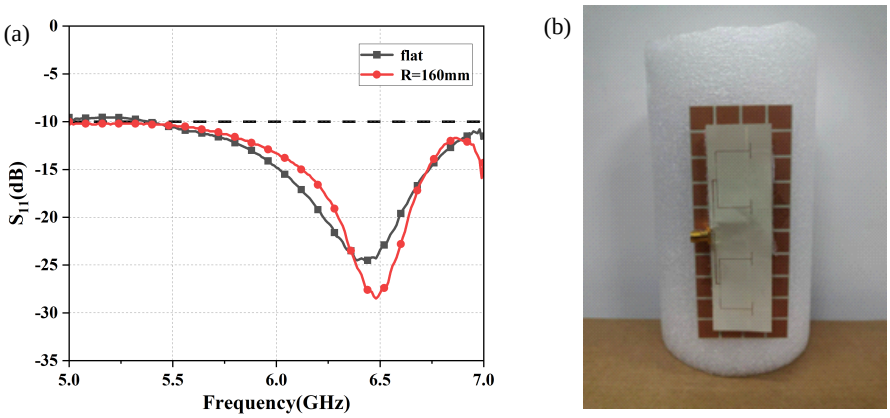

FIGURE 18. Measured S_{11} of the integrated antenna bending along the cylinder. (a) S_{11} parameter. (b) Experimental setup.

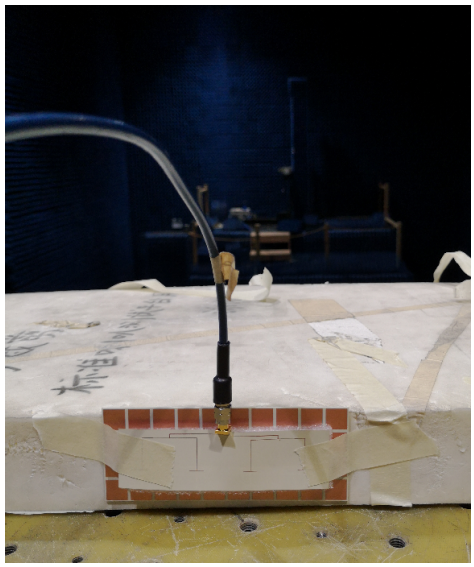

FIGURE 19. Anechoic room testing.

sured radiation patterns at 6.5 GHz is provided in Figure 20, showing a strong correlation between the two sets of results. A notable reduction in backward radiation is observed after introducing the AMC reflector, as evidenced by a significant improvement in the FBR. The integration of the AMC results in notable side-lobe suppression. The simulated side-lobe level on the H-plane is less than -20.51 dB, and the measured side-lobe level is less than -18.5 dB, while the overall trend is the same.

Figure 21 presents the performance of the proposed antenna with and without an AMC reflector. In Figure 21(a), the measured gain deviates from the simulation by 0.55 dB. This error is well within the 3 dB margin and is considered acceptable in engineering practice. The maximum gain within the measured frequency band is 13.8 dBi. Compared to the antenna without the AMC reflector, the measured gain shows an improvement of 3.3 dB, indicating a significant enhancement. Figure 21(b) shows the comparison of the FBR of the antenna with and without the AMC reflector. Without the AMC reflector, the maximum FBR of the antenna is 2.81 dB, while with the AMC reflector, it increases to 25.3 dB.

3.3. SAR Evaluation

The radiation from a wearable antenna operating near the body poses risks to human tissues when the energy absorption exceeds certain limits. SAR is a key metric for quantifying human exposure to electromagnetic radiation. The corresponding calculation formula for the SAR value is given by equation:

$$SAR = \frac{\sigma |E_i|}{\rho} \tag{4}$$

where E_i denotes the induced electric field, and σ and ρ represent the conductivity (s/m) and mass density (kg/m^3) of the tissue, respectively.

Figure 22 shows the simplified human body simulation model in High Frequency Structure Simulator (HFSS). The distance H represents the spacing between the antenna system and this model. The human tissue model consists of four distinct layers: a 2 mm skin layer, a 5 mm fat layer, a 20 mm muscle layer, and a 13 mm bone layer. Table 3 summarizes the electromagnetic parameters of each layer in the human tissue model. Table 4 presents SAR values at various H. The simulation results show that at 6.5 GHz, with H set to 2 mm, the SAR value is 0.05 W/kg/10 g, which is well below the EU standard of 2 W/kg/10 g for tissues. It means that the radiation energy from the antenna has a minimal effect on human tissue.

TABLE 3. Electromagnetic properties of various human tissues.

	Skin	Fat	Muscle	Bone
ε_r	37.95	5.27	52.67	18.49
σ (S/m)	1.49	0.11	1.77	0.82
Density (kg/m^3)	1001	900	1006	1008
Thickness (mm)	2	5	20	13

4. PERFORMANCE COMPARISON

Table 5 compares the performance of the proposed antenna with several previously reported designs. In [10, 15, 17, 20–22], the proposed antenna has better performances than other antennas

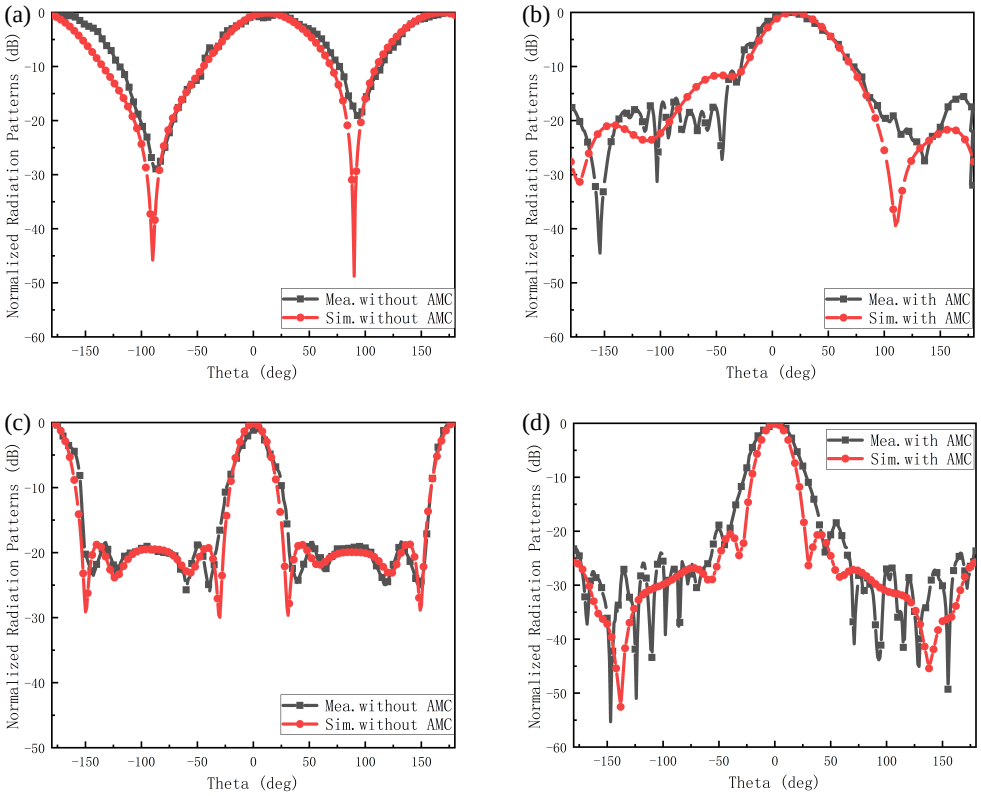

FIGURE 20. The measured and simulated radiation patterns at 6.5 GHz. (a) yoz-plane without AMC. (b) yoz-plane with AMC. (c) xoz-plane without AMC. (d) xoz-plane with AMC.

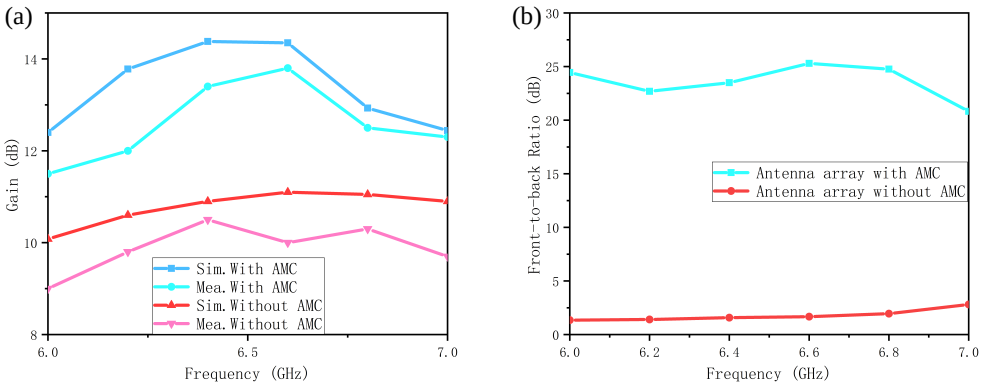

FIGURE 21. Performance comparison of the proposed antenna with and without AMC reflector. (a) Gain. (b) FBR.

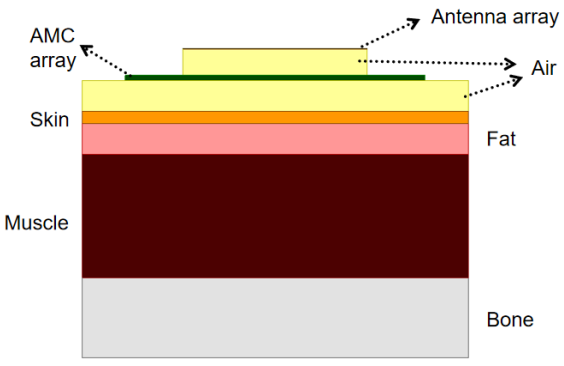

FIGURE 22. Human body simulation model.

TABLE 4. Maximum SAR values at various H.

Central Frequency (GHz)	H (mm)	Average SAR (W/Kg/10)
6.5	2	0.05
6.5	3	0.05
6.5	5	0.042

in terms of gain, FBR, and side-lobe level. In [19], the bandwidth of the antenna is narrow, and the gain is 12.03 dBi. Compared to above antennas, the presented antenna offers higher gain, better FBR, and lower sidelobe level. Therefore, the antenna has good wearable application prospects.

TABLE 5. Comparison of antenna performance.

Ref.	Size (mm^2)	Bandwidth (GHz)	Substrate	Flexibility	FBR (dB)	Sidelobe (dB)	Gain (dBi)	Efficiency (%)
[10]	60×60	2.39–2.48 (4%)	Denim	Flexible	13.82	–	6.75	> 65
[15]	75×90	2.63–6 (78.1%)	Roger RT5880, FR4	Rigid	–	–	11.5	> 51
[17]	76×76	2–2.6 (26.1%)	Felt	Flexible	–	–	6.57	> 72.22
[19]	137×45.9	5.62–6 (6.5%)	LCP	Flexible	26.04	–	12.03	> 80
[20]	166×66	3.5–5.8 (49.5%)	FR4	Rigid	–	–	12.4	> 77.5
[21]	170×70	4.5–6.5 (36.4%)	PI, PDMS	Flexible	–	-12	11.8–13.6	> 75
[22]	144×48	5.25–6.06 (14.3%)	F4BM 220	Flexible	–	–	7.9	–
This work	122×48.8	5.6–6.8 (19.35%)	LCP, Rogers 4003	Flexible/ Semi-Flexible	25.3	-18.5	13.8	80

5. CONCLUSION

In this paper, an antenna array integrated with an AMC reflector is proposed for high gain, low-side-lobe levels, and low SAR. After backing with the AMC reflector, the antenna operating bandwidth is 5.6–6.8 GHz; the measured maximum gain reaches 13.8 dBi; and the FBR is 25.3 dB. The simulation side-lobe level reaches -20.51 dB, while the measured side-lobe level is -18.5 dB. When the antenna array is on the human body model, the SAR is only 0.05 W/kg. With above good characteristics, the proposed antenna is suitable for wearable applications.

REFERENCES

[1] Vaezi, M., A. Azari, S. R. Khosravirad, M. Shirvanimoghaddam, M. M. Azari, D. Chasaki, and P. Popovski, "Cellular, wide-area, and non-terrestrial IoT: A survey on 5G advances and the road toward 6G," *IEEE Communications Surveys & Tutorials*, Vol. 24, No. 2, 1117–1174, 2022.

[2] Fraire, J. A., O. Iova, and F. Valois, "Space-terrestrial integrated Internet of Things: Challenges and opportunities," *IEEE Communications Magazine*, Vol. 60, No. 12, 64–70, 2022.

[3] Azari, M. M., S. Solanki, S. Chatzinotas, O. Kodheli, H. Sallouha, A. Colpaert, J. F. M. Montoya, S. Pollin, A. Haqiqatnejad, A. Mostaani, E. Lagunas, and B. Ottersten, "Evolution of non-terrestrial networks from 5G to 6G: A survey," *IEEE Communications Surveys & Tutorials*, Vol. 24, No. 4, 2633–2672, 2022.

[4] Taleb, R. D., M. Z. Baba-Ahmed, and M. A. Rabah, "Reconfigurable graphene antenna for a network cognitive radio: A novel solution for X-band satellite communications," *Advances in Space Research*, Vol. 73, No. 9, 4742–4750, 2024.

[5] Algaba-Brazález, A., P. Castillo-Tapia, M. C. Viganó, and O. Quevedo-Teruel, "Lenses combined with array antennas for the next generation of terrestrial and satellite communication systems," *IEEE Communications Magazine*, Vol. 62, No. 9, 176–182, 2024.

[6] Rao, N. and V. D. Kumar, "Miniaturization of microstrip patch antenna for satellite communication: A novel fractal geometry approach," *Wireless Personal Communications*, Vol. 97, No. 3, 3673–3683, 2017.

[7] Zhu, X. and C. Jiang, "Creating efficient integrated satellite-terrestrial networks in the 6G era," *IEEE Wireless Communications*, Vol. 29, No. 4, 154–160, 2022.

[8] Wang, J., C. Jiang, L. Kuang, and R. Han, "Satellite multi-beam collaborative scheduling in satellite aviation communications," *IEEE Transactions on Wireless Communications*, Vol. 23, No. 3, 2097–2111, 2024.

[9] Yang, S., J. An, Y. Xiu, W. Lyu, B. Ning, Z. Zhang, M. Debbah, and C. Yuen, "Flexible antenna arrays for wireless communications: Modeling and performance evaluation," *IEEE Transactions on Wireless Communications*, Vol. 24, No. 6, 4937–4951, 2025.

[10] Nie, H.-K., X.-W. Xuan, Q. Shi, A. Guo, M.-J. Li, H.-J. Li, and G.-J. Ren, "Wearable antenna sensor based on EBG structure for cervical curvature monitoring," *IEEE Sensors Journal*, Vol. 22, No. 1, 315–323, 2022.

[11] Kumkhet, B., P. Rakluea, N. Wongsin, P. Sangmahamad, W. Thaiwirot, C. Mahatthanajatuphat, and N. Chudpooti, "SAR reduction using dual band EBG method based on MIMO wearable antenna for WBAN applications," *AEU — International Journal of Electronics and Communications*, Vol. 160, 154525, 2023.

[12] Wajid, A., A. Ahmad, S. Ullah, D.-y. Choi, and F. U. Islam, "Performance analysis of wearable dual-band patch antenna based on EBG and SRR surfaces," *Sensors*, Vol. 22, No. 14, 5208, 2022.

[13] Ashyap, A., R. Raad, F. Tubbal, W. A. Khan, and S. Abulgasem, "Highly bendable AMC-based antenna for wearable applications," *IEEE Access*, Vol. 12, 154 195–154 211, 2024.

[14] Wang, S. and H. Gao, "A dual-band wearable conformal antenna based on artificial magnetic conductor," *International Journal of Antennas and Propagation*, Vol. 2022, No. 1, 9970477, 2022.

[15] Nguyen, N.-L., C. D. Bui, and Q. S. Nguyen, "Design of a compact antenna with broadband and high gain," *Electromagnetics*, Vol. 44, No. 1, 18–31, 2024.

[16] Saha, P., D. Mitra, and S. K. Parui, "Control of gain and SAR for wearable antenna using AMC structure," *Radioengineering*, Vol. 30, No. 1, 81–88, 2021.

[17] Youssef, O. M., M. E. Atrash, and M. A. Abdalla, "A compact fully fabric I-shaped antenna supported with textile-based AMC for low SAR 2.45 GHz wearable applications," *Microwave and Optical Technology Letters*, Vol. 65, No. 7, 2021–2030, 2023.

[18] Yang, S., C. Yu, X. Yang, and J. Zhao, "A tri-band flexible antenna based on tri-band AMC reflector for gain enhancement and SAR reduction," *AEU — International Journal of Electronics and Communications*, Vol. 168, 154715, 2023.

[19] Chu, J., C. Du, and H. Shu, "A high FBR low SAR and AMC-backed compact wearable antenna array for WBAN applica-

tions," *International Journal of Microwave and Wireless Technologies*, Vol. 16, No. 9, 1499–1509, 2024.

[20] Alwareth, H., I. M. Ibrahim, Z. Zakaria, A. J. A. Al-Gburi, S. Ahmed, and Z. A. Nasser, "A wideband high-gain microstrip array antenna integrated with frequency-selective surface for Sub-6 GHz 5G applications," *Micromachines*, Vol. 13, No. 8, 1215, 2022.

[21] Zu, H., B. Wu, P. Yang, W. Li, and J. Liu, "Wideband and high-gain wearable antenna array with specific absorption rate suppression," *Electronics*, Vol. 10, No. 17, 2056, 2021.

[22] Huang, R. and X. Liu, "A wearable low-profile flexible dual-polarized antenna array loaded with AMC for 5 GHz WLAN on-/off-body applications," in *2022 IEEE MTT-S International Microwave Workshop Series on Advanced Materials and Processes for RF and THz Applications (IMWS-AMP)*, 1–3, Guangzhou, China, 2022.